NUMERICAL SIMULATION OF CONDENSATION IN BUBBLY FLOW

P. Ruyer[1], K. Keshk[2], F. Deffayet[1], Ch. Morel[3], J. Pouvreau[3], F. François[3].

1. IRSN DPAM, CE Cadarache, BP 13115 St Paul lez Durance Cedex, France
2. CRIT-Interim, France
3. CEA Grenoble, 17 rue des martyrs, 38054 Grenoble Cedex 9

Abstract
In the framework of safety studies of Pressurized Water Reactors, boiling bubbly flow and Departure from Nucleate Boiling are now investigated at the CFD scale in particular with the NEPTUNE_CFD code developed in the framework of the NEPTUNE project, financially supported by the Commissariat à l'Énergie Atomique (CEA), Électricité de France (EDF), the Institut de Radioprotection et de Sûreté Nucléaire (IRSN) and AREVA-NP. The prediction of subcooled convective boiling flows throughout PWR assemblies relies on both prediction of nucleation of bubbles in the wall region and of their life time in the core flow where subcooled liquid may induce condensation. In the perspective of validation of CFD simulations of convective nucleate boiling flows, there is a need of assessing both boiling and condensation independently. This study contributes to the validation of the NEPTUNE_CFD code concerning liquid-vapour bubbly flows. It focuses on the subcooled flows with condensation but in the absence of wall heat transfer. Some of the data incoming from the TESS experimental program are used to perform the numerical simulations. Conclusion are drawn concerning the sensitivity of the results with regard to the models for *(i)* bubble migration from wall to core, and *(ii)* interfacial heat transfers that result in bubbles condensation. This work is a first step toward a more extensive validation against the whole TESS tests matrix.

1. INTRODUCTION

The use of the CFD of two-phase boiling bubbly flows for the purpose of safety studies is nowadays under investigation, in particular in the frame of the French "Institut de Radioprotection et de Sûreté Nucléaire" (IRSN) research program on nuclear fuel safety. The ability and validity of CFD calculations to simulate those type of flows has already been the subject of several studies, *e.g.* (Morel and Laviéville, 2008). One of the specificity of this boiling regime relies on the coexistence of several heat and mass transfer processes. In a pipe section, on the one hand, the nucleate boiling process generates a vaporization rate near the wall, whereas, on the other hand, cold liquid, at the centre of the pipe, condenses the bubbles. Bubble dynamics is then a key issue to describe the migration of vapour from wall to core flow. Moreover coalescence and possible fragmentation of the bubbles may modify the size distribution of the bubble population and consequently the intensity of interfacial transfers. At the CFD scale, each of these mechanisms needs to be described by corresponding momentum, heat and mass transfers laws, and each of these laws would ideally require a specific, separate effect, validation. The model of the nucleate boiling process at the CFD scale is certainly the most difficult to describe, in particular because one can not study this process independently from the others, and some improvements in the description of the physical processes at small scale are still under way, see (Basu *et al.* 2005). Bubble dynamics has been the subject of a large amount of experimental and numerical studies, either at the scale of the single bubble dynamics or for most complex cases like populations of bubbles with a polydispersion in size, *e.g.* (Morel *et al.* 2010). This dynamics can be more easily studied as an independent process because one can deal with adiabatic flows of incondensable bubbles.
In this paper, we address the condensation process through both experimental and numerical studies. The main difficulty relies on the ability of characterizing the single phenomenon of condensation throughout both the experimental results and its numerical modelling. The TESS facility at CEA Grenoble provides a data base for the study of boiling convective bubbly flows in a vertical pipe without wall transfer. In part 2, we address the description of the facility, the different measurements that it provides as well as the tests matrix. In part 3, we present the set of closure laws of the two-fluid model related to the description of condensation in convective bubbly flows. We also give the main

numerical settings that we use for the simulations with the NEPTUNE_CFD code, (Guelfi *et al* . 2007). In part 4, we study the sensitivity of the numerical solution to some modelling issues and analyze comparison with experimental data.

2. DESCRIPTION OF THE TESS EXPERIMENTAL PROGRAM

2.1 General description of the loop

The goal of the set of experiments of the TESS program is to finely characterize a convective bubbly flow that experiences condensation. For this purpose, a liquid-vapour boiling ascending flow is generated throughout a vertical cylindrical pipe. Subcooled liquid is injected at the bottom of the pipe and flows along electrically heated walls. The wall heat transfer corresponds to nucleate boiling regime and bubbles are formed along the wall. Vapour volumetric fraction increases along the flow and near-wall liquid is heated up. The investigated flow lies downstream this heated part, where the pipe walls are adiabatic. In this upper part, we thus have a convective bubbly flow, the liquid temperature being below saturation. Condensation will thus be one of the leading phenomena for the evolution of the bubble volumetric fraction.

The test section is a vertical cylindrical pipe made of Inconel 600, of internal and external diameters of respectively 19.2 mm and 21.2 mm and of 4 m of total length. The fluid is a HFC-134a and experiments are performed over 27 different thermal-hydraulic conditions and for a wide range of pressure P, specific velocity G, liquid subcooling (Te-Tsat) and heating power W. The typical ranges of variations of the parameters are provided on Tab 1.

Table 1: Ranges of thermal-hydraulic conditions

	Min	Max		Min	Max
P	10 bar	30 bar	G	700 $kgm^{-2}s^{-1}$	4500 $kgm^{-2}s^{-1}$
Te	293K	~Tsat(P)	W	-	100 kW

The domain of application considered concerns the study of boiling bubbly flows of water at 155 bars throughout typical PWR assemblies. The pipe diameter is close to the hydraulic diameter of a typical subchannel between four rods. By using HFC-134a, one is able to recover some typical PWR two-phase flow conditions (in particular in terms of vapour volumetric fraction, density ratio between vapour and liquid, Jakob and Reynolds numbers) with a lower level of pressure and heating power (in particular in order to approach the critical heat flux conditions).

The measurements are made at different elevations downstream the heated part (at 4 or 5 elevations depending on the test considered, z=0; 0.025; 0.075; 0.1; 0.175 m, the reference corresponding to the top of the heated part). For each elevation, the probes are moved over a whole diameter (around 50 measurements on a diameter). Fig. 1 provides a schematic view of the system used to vary the radial position of the probes. A two-tip optical probe, of 20µm individual diameter at the tip and of 125µm radial spacing, provides two temporal signals characterizing the presence of the phases at two positions slightly shifted in the axial direction (550µm). Volumetric vapour fraction, interfacial velocity, bubble size distribution (from which Sauter mean diameter or interfacial area concentration can be deduced) are deduced from these signals thanks to a statistical treatment (Cubizolles, 1996). The accuracy of these measurements is of ±0.02 on void fraction value, ±10%[1] on interfacial velocity, ±10% on interfacial area density, ±12% on Sauter mean diameter. A thermocouple of 250µm diameter allows to determine the liquid temperature with an accuracy of 0.3K (Gnemmi et al. 2008) at an axial distance of 12.5mm of the optical probe. This provides a finely resolved radial and axial map of the two-phase flow.

For each position of the probe, a specific run of the loop needs to be performed, and thus the measurements corresponding to a given set of control parameters of the loop, *i.e.* thermal-hydraulic conditions corresponds actually to a set of runs. The variations of the control parameters over these runs has been ensured to be very low. Moreover for a set of thermal-hydraulic conditions, the set of data has been reproduced at two different dates with good accuracy. The two test cases considered in this paper correspond to the control parameters summarized in table 2.

[1] relative accuracy is prescribed in %.

Table 2: Table of experimental conditions

Test n°	Flow rate ($kg\ m^{-2}s^{-1}$)	Pressure (bar)	Wall heat-flux ($W\ m^{-2}$)	Inlet temperature (K)
1	1950	26.6	$4\ 10^4$	346
2	2660	14.6	$2\ 10^5$	302

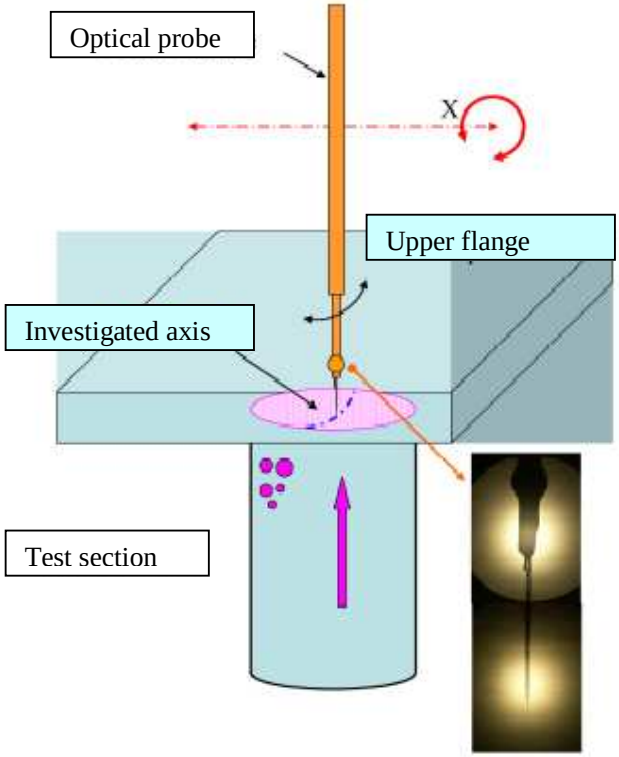

Fig. 1 : Schematic representation of the instrumentation device for radial profiles

3. NUMERICAL MODELLING

The numerical simulations are performed thanks to the NEPTUNE_CFD code. The two-fluid one-pressure model equations are solved using an elliptic approach, as well as a finite volume method and a collocated arrangement for all variables. Let us introduce the set of equations and closure laws that we considered in this study.

3.1 Two-fluid model closure relations

The mass, momentum and enthalpy balance equations of the two-fluid model read (Ishii and Hibiki, 2006):

$$\frac{\partial \alpha_k \rho_k}{\partial t} + \nabla.(\alpha_k \rho_k \underline{V}_k) = \Gamma_k \qquad k = L, G$$

$$\frac{\partial \alpha_k \rho_k \underline{V}_k}{\partial t} + \nabla.(\alpha_k \rho_k \underline{V}_k \underline{V}_k) = -\alpha_k \underline{\nabla} p_k + \underline{M}_k + \Gamma_k \underline{U^I}_k + \alpha_k \rho_k \underline{g} + \nabla.\left[\alpha_k \left(\underline{\underline{\tau}}_k + \underline{\underline{\tau}}_k^T\right)\right] \qquad k = L, G \quad (1)$$

$$\frac{\partial \alpha_k \rho_k H_k}{\partial t} + \nabla.(\alpha_k \rho_k H_k \underline{V}_k) = -\nabla.(\alpha_k \underline{Q}_k) + \alpha_k \frac{\partial p_k}{\partial t} + \Pi_k + \varphi_w + \alpha_k \rho_k \underline{V}_k \underline{g} + \nabla.(\alpha_k \underline{V}_k \underline{\underline{\tau}}_k) + \underline{M}_k \underline{V}_k \qquad k = L, G$$

where α_k is the local time-fraction of presence of phase k, ρ_k its averaged density, V_k its averaged velocity, H_k its averaged total specific enthalpy (*i.e.* the sum of the specific enthalpy and kinetic energy) and p_k the bulk-averaged pressure for phase k. Γ_k, is the interfacial mass transfer rate, the vector g is the gravity acceleration, τ_k and τ_k^T are the averaged viscous stress tensor and the turbulent "Reynolds" stress tensor, respectively, the vector M_k is the averaged interfacial transfer of momentum,

Q_k is the heat flux vector, Π_k the volumetric interfacial enthalpy transfer, and φ_w the wall heat flux. The phase index k takes the values L for the liquid phase and G for the gas phase. In the enthalpy balance equations, the terms corresponding to the contribution of gravity, stress and interfacial momentum transfers (second line of the right hand side of the equation (1)) are neglected in this study, because they are of second order with respect to heat and mass transfers. Moreover, since we will deal with adiabatic walls, the heat flux φ_w will be set to zero. Eqs. (1) have been obtained by (Ishii and Hibiki 2006) by means of a time-averaging, but very similar equations can be obtained by means of ensemble averaging *e.g.* (Drew and Passman, 1999). The difference between the interfacial-averaged pressure for phase k p_k^i and the bulk-averaged pressure p_k has been neglected. We will also neglect the difference between the two bulk-averaged pressures in the two phases, therefore making the approximation $p_L = p_G = p$. Making this approximation of a common pressure for the two phases, the closure issue of the system of equations (1) lies in the averaged viscous stress tensors for the two phases, the Reynolds stress tensors for the two phases and the interfacial momentum, heat and mass transfers. The Reynolds stress tensor for the continuous liquid phase is determined thanks to a k-ε model, whereas the turbulent dispersion of the dispersed vapour phase (bubbles) is considered through an additional interfacial momentum transfer term. Hereafter we describe more precisely the closure of these last terms concerning interfacial transfers.

Interfacial momentum transfers:

If we neglect the averaged effects of the interfacial tension, the averaged interfacial momentum balance reduces to (Ishii and Hibiki, 2006):

$$\sum_{k=L,G} \underline{M}_k = 0 \qquad (2)$$

Therefore it is sufficient to express the gas (or liquid) interfacial momentum transfer term, the liquid (or gas) interfacial momentum transfer being deduced from the action and reaction principle, in the context of the assumptions mentioned above. In bubbly flow studies, the interfacial momentum transfer term M_k is often decomposed into several averaged forces, namely a drag force, an added mass force, a lift force, a turbulent dispersion force and sometimes a wall force. The physical models considered in this study are the (Ishii, 1990) coefficient for the drag force, the (Zuber, 1964) coefficient for the added mass, and the (Lance and Lopez de Bertodano, 1994) model for the turbulent dispersion force. Lift (Auton 1987) and wall (Tomiyama, 1998) forces act mainly in the near wall region. We will study the sensitivity of the results according to these closure relations.

Interfacial heat and mass transfers:

These transfers are closely related and they govern the dynamics of condensation that is the main focus of this study. Let us introduce the three basic relations for their modelling as being the two heat transfers between the phases and the interface and the heat balance at the interface. In the frame of the model used, the interface is not tracked. The assumption for the vapour phase to be made of spherical bubbles of given diameter, say D (m), allows to define the local interfacial area density, say a_i (m^{-1}), as

$$a_i = \frac{6\alpha_G}{D} \qquad (3)$$

The interface is assumed to be at thermodynamic equilibrium, it is thus at saturation temperature, say T_{sat}, of the local pressure.

We consider that the bubbles are created with vapour at saturation temperature, and the heat transfer between the bubbles core and the interface is a simple numerical relaxation toward this thermal equilibrium. For a given volumetric interfacial mass transfer rate Γ_G (kg s^{-1} m^{-3}), there is a corresponding transfer $\Gamma_G H_G^I$ in the enthalpy balance, where H_G^I (J kg^{-1}) reads for the specific enthalpy of either created, or, in our case, condensed vapour. The total volumetric interfacial enthalpy transfer on the vapour side, Π_G (Wm^{-3}), thus reads

$$\Pi_G = \frac{\alpha_G \rho_G C_{p,G}}{\theta}\left(T_{sat} - T_G\right) + \Gamma_G H_G^I \qquad (4)$$

where, $C_{p,G}$ (J kg^{-1} K^{-1}) is the specific heat capacity of the vapour phase, T_G (K) its temperature, and the time θ (s) an arbitrary small constant. In practice, since the vapour temperature is always close to saturation, the heat transfer is negligible and the enthalpy transfer reduces to the mass transfer part, i.e.

$$\Pi_G \approx \Gamma_G H_{sat,G} \qquad (5)$$

On the liquid side, the interfacial heat transfer is evaluated thanks to an analogy with the transfer between a sphere of diameter D and surface temperature T_{sat} and a flow at the liquid temperature T_L and velocity V_R, V_R being the norm of the relative velocity of the liquid phase with respect to the vapour phase, *i.e.* $V_R=|V_L-V_G|$. The correlation of (Ranz and Marshall 1952) is used for this evaluation. The interfacial enthalpy transfer related to liquid mass transfer $\Gamma_L=-\Gamma_G$, considers the specific enthalpy, H_L^I, of the liquid created by condensation. The volumetric enthalpy transfer on the liquid side, Π_L (Wm-3), thus reads

$$\Pi_L = \frac{a_i\, Nu\, \lambda_L}{D}\left(T_{sat} - T_L\right) + \Gamma_L H_L^I \tag{6}$$

Where λ_L is the thermal conductivity of the liquid and the Nusselt number Nu of the Ranz and Marshall correlation reads as a function of the bubble Reynolds number Re and the liquid Prandtl number Pr:

$$Nu = 2 + 0.6\,\mathrm{Re}^{0.5}\,\mathrm{Pr}^{0.33}, \qquad \mathrm{Re} = \frac{\rho_L D V_R}{\mu_L}, \quad \mathrm{Pr} = \frac{\mu_L C_{p,L}}{\lambda_L} \tag{7}$$

μ_L being the dynamic viscosity of the liquid and $C_{p,L}$ its specific heat capacity.

The interfacial heat balance is a constitutive relation of the two-fluid model incoming from an averaged writing of the interfacial jump condition on energy where kinetic energy fluxes and viscous dissipation have been neglected. It thus reads $\Pi_L=-\Pi_G$. Using the expressions (6) and (4), it yields to the following relation between the heat transfer from both side of the interface and the interfacial mass transfer rate

$$\Gamma_G\left(H_L^I - H_G^I\right) = \frac{a_i\, Nu\, \lambda_L}{D}\left(T_{sat} - T_L\right) + \frac{\alpha_G \rho_G C_{p,G}}{\theta}\left(T_{sat} - T_G\right) \tag{8}$$

in the frame of a local and instantaneous level of description of the interface dynamics. In our case, we can write

$$\Gamma_G\left[\left(H_L^I - H_{sat,L}\right) + \underbrace{\left(H_{sat,L} - H_{sat,G}\right)}_{\Lambda}\right] \approx \frac{a_i\, Nu\, \lambda_L}{D}\left(T_{sat} - T_L\right) \tag{9}$$

Where Λ is the specific latent heat for the condensation. The specific enthalpy of the liquid created by condensation H_L^I is a variable incoming from the two-phase averaging procedure that lies behind the establishment of the two-fluid model and needs for specific closure. Two extreme cases can be considered:

- either we assume that the liquid enthalpy flux incoming from the interfacial liquid boundary (corresponding to the liquid mass flux created by condensation) bears the enthalpy of this boundary, namely the saturation value. In this case, we write $H_L^I=H_{sat,L}$ and the first term of the left hand side of (9) is zero.
- or, we assume that the liquid created very well mix with the liquid surrounding the bubbles, adopting instantaneously its enthalpy, in which case, we write $H_L^I=H_L(T_L,p)$ and the interfacial heat transfer has to contribute to both condensation of the vapour phase and cooling of the liquid from T_{sat} to T_L.

It is worth pointing out that *(i)* both cases satisfy an equivalent global energy balance and differences only affect the kinetics of the condensation process, *(ii)* this distinction only plays a role when liquid subcooling, namely the difference $(T_{sat}-T_L)$ is sufficiently large and *(iii)* that the correct representation of the interfacial heat balance at the averaged scale of the two-fluid model lies between these two cases. We'd like to emphasize the fact that the modelling of the condensation process, not only relies on the choice for the interfacial heat transfer correlation, but also on this interfacial enthalpy modelling.

3.2 Numerical settings

Calculations are made on the mesh of a slice (an angular sector of 10°) of the cylindrical pipe thanks to the axi-symmetry of the test section. Independency of the obtained results to this simplification has been insured by comparing the results with calculations over the whole (360°) pipe section. The computational domain has a single cell azimuthally, and a mesh size of 0.5mm in the radial direction and of 7.5mm in the vertical direction. No sensitivity to mesh refinement in both radial and vertical

direction has been observed for calculations with a number of cells multiply by 2 or 4 in both radial and axial directions. The boundary conditions reflect the symmetry on the faces at the centre of the pipe and azimuthally. Outlet boundary conditions are considered at the top of the calculation domain that allows to prescribe the pressure level.

At the lower boundary of the calculation domain, say the inlet plane, we impose as boundary conditions the experimental data corresponding to the level "z=0m". This concerns the radial profiles of the liquid temperature, bubbles velocity and volumetric fraction. The bubbles temperature is imposed to be the saturation temperature at the local pressure. The liquid velocity as well as the liquid turbulent kinetic energy and dissipation rate of the kinetic energy remain to be prescribed without experimental values. This is the object of the first sensitivity study.

As far as the test 1 data are concerned, the value of the experimental Sauter diameter lies in the range [0.25mm; 0.35mm] over the whole domain. The bubble size of 0.3 mm is thus chosen as a uniform parameter over the whole computational domain. This is an interesting simplification with regard to a more elaborate model for the bubble size evolution that often requires an additional transport equation (or set of transport equations), *e.g.* the interfacial area density transport equation. This simplicity certainly hides a more complex process in the flow: condensation, that naturally drives to the decrease of individual bubble size is apparently balanced by coalescence that shifts bubble size distribution toward larger diameters. In other words, the decrease of the vapour volumetric fraction, while the Sauter diameter is kept constant, implies a decrease in the volumetric number of bubbles. It would be interesting to study the ability of the models for bubble size distribution to reproduce the observed evolution of the Sauter diameter through the calculation of both coalescence and condensation effects on size distribution.

4. NUMERICAL RESULTS

4.1 Influence of the liquid velocity and turbulent fields inlet boundary conditions

We consider the numerical simulation corresponding to the conditions of test 1 (*cf.* Table 2). The inlet liquid velocity is one of the unknown of the set of parameters for the simulation. To generate this boundary condition, we consider *(i)* a profile deduced from the bubble velocity experimental one, considering a uniform (along the pipe diameter) relative velocity, *(ii)* an established profile deduced from a numerical calculation of liquid flow over a very long pipe of same diameter. Both satisfy the correct inlet mass flow rate that is one of the experimental loop control parameter. The two profiles are illustrated in Fig. 2. The two profiles are very different in particular in terms of wall shear stress.

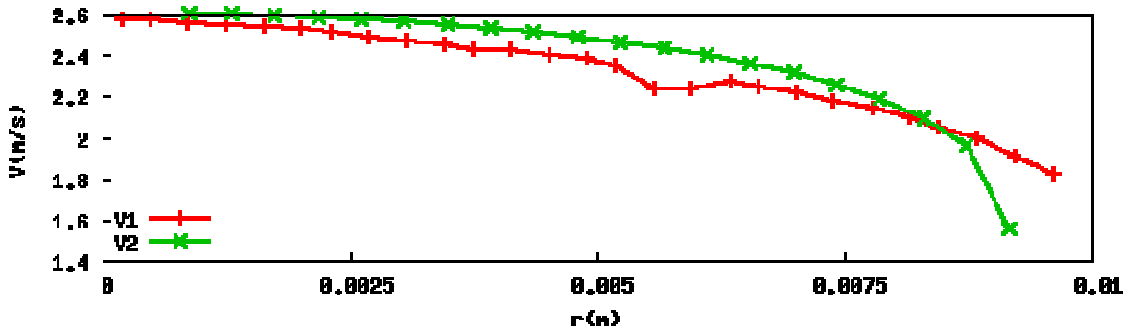

Fig. 2 : Liquid velocity profiles at the inlet of the simulated domain : V1 corresponds to the profile that can be deduced from the vapour bubble velocity experimental profile at z=0m, V2 to the numerical profile obtained after establishment of the flow

Using V1 profile at the z=0m elevation, the liquid velocity profile evolves along the pipe toward the V2 shape. Some typical vapour volumetric fraction radial profiles at different elevations in the pipe are represented on Fig. 3 according to the two different types of inlet boundary conditions for the liquid velocity field and for the conditions of the experimental test n°1.They show large differences in particular in the near wall region. Actually, the establishment of the liquid flow in the V1 case induces a sharp decrease of liquid velocity close to the wall that leads to specific bubbles dynamics (through drag and lift forces), in particular near the wall where they are more concentrated. Therefore, when the V1 profile is used, the evolution of vapour volumetric fraction is governed by the near-wall (larger

radius) liquid dynamics and it leads to inconsistent results and thus deserves the interest of comparison with experimental data. When the numerical profile V2 is used the evolution of the radial distribution is more progressive. V2 profile will thus be used for all further simulations considered in the present study. It is worth pointing out that we also considered the liquid turbulent kinetic energy and dissipation rate profiles at the outlet of the long pipe calculation as inlet boundary conditions. Otherwise (*i.e.* using flat inlet profiles for these quantities) the vapour volumetric fraction remains governed by inlet effect (even though it is less perturbed than in the V1 case). For information, the corresponding liquid turbulent kinetic energy is of the order of one percent of the liquid kinetic energy at inlet.

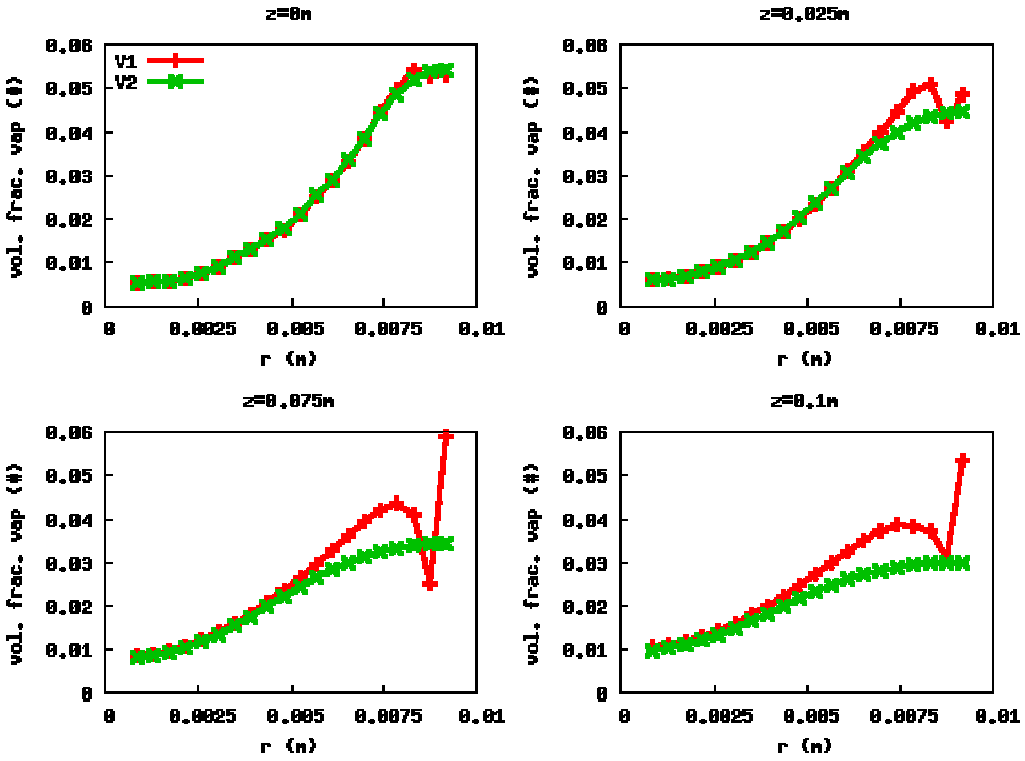

Fig. 3: Vapour volumetric fraction radial profiles at different elevations for two types of liquid velocity radial profiles as inlet boundary conditions

4. 2 Axial evolution of the vapour volumetric fraction profile : main phenomenon

In the "V2" case, let us analyze vapour volumetric fraction evolution with increasing elevation. Since bubbles have been generated upstream z=0m by wall nucleation, the profile at z=0m has a peak at the wall. The averaged vapour volumetric fraction over a cross section decreases with increasing inlet distance. The vapour velocity remaining of the same order of magnitude, this corresponds to condensation. Analysis of the intensity of condensation rate shows that this is maximal at mid-position between wall and centre, a place where there are both cold liquid and bubbles. This is consistent with equation (8) that shows that condensation rate is maximal where the product $a_i(T_L-T_{sat})$ is maximal. Indeed, near the wall, despite high concentration of bubbles, the liquid temperature is close to saturation, since it has been heated upstream, whereas at the centre there is very few bubbles.

The axial evolution of the vapour volumetric fraction profile shows a flattening of radial variation through both an increase of the volumetric fraction at the centre of the pipe and a decrease near the wall. This is due to radial migration of bubbles under the influence of several mechanisms, namely the hydrodynamic forces acting on individual bubbles and the turbulent dispersion of the population that tends to reduce volumetric fraction gradients. We now study the sensitivity of the results to this modelling issue.

4. 3 Sensitivity of the results to the closure laws for bubble dynamics

The turbulent dispersion force tends to smooth the gradient of vapour volumetric fraction, and thus in our case is the driving force for the migration toward the centre of the pipe. The contribution M^L of the lift force on bubbles in the interfacial momentum transfer reads

$$\underline{M_G^L} = -\underline{M_L^L} = -C_L\,\alpha_G\,\rho_L\left(\underline{V_G} - \underline{V_L}\right)\wedge\left(\underline{\nabla}\wedge\underline{V_L}\right)$$

Where C_L is a coefficient that we take equal to 0.29. In a vertical upward pipe flow, this acts in pushing the bubbles toward the wall, thus in opposite direction to the turbulent dispersion. An additional force is often considered in the frame of the two-fluid model. It has been introduced to describe the dynamics of bubbles through the liquid boundary layer that acts to limit the bubble concentration in this region. The corresponding interfacial momentum transfer reads

$$\underline{M_G^W} = -\underline{M_L^W} = -C_W\,\alpha_G\,\rho_L\left[\left(\underline{V_G} - \underline{V_L}\right) - \left(\left(\underline{V_G} - \underline{V_L}\right)\bullet\underline{n}\right)\underline{n}\right]^2\underline{n}\,\frac{D}{2}\left(\frac{1}{y^2} - \frac{1}{\left(\Theta - y^2\right)}\right)$$

where C_W is a coefficient, n the vector normal to the wall, y the distance to the wall and Θ the pipe diameter. (Tomiyama, 1998) provides a correlation for C_W valid for Eötvös number, say E_O, values greater than 1 (the Eötvös number reads $E_O=(\rho_L-\rho_G)\,g\,D^2/\sigma$, where σ is the surface tension, and quantifies the ability of the bubble to be non-spherical). In our case, E_O=0.45 and we took the C_W value for E_O=1.

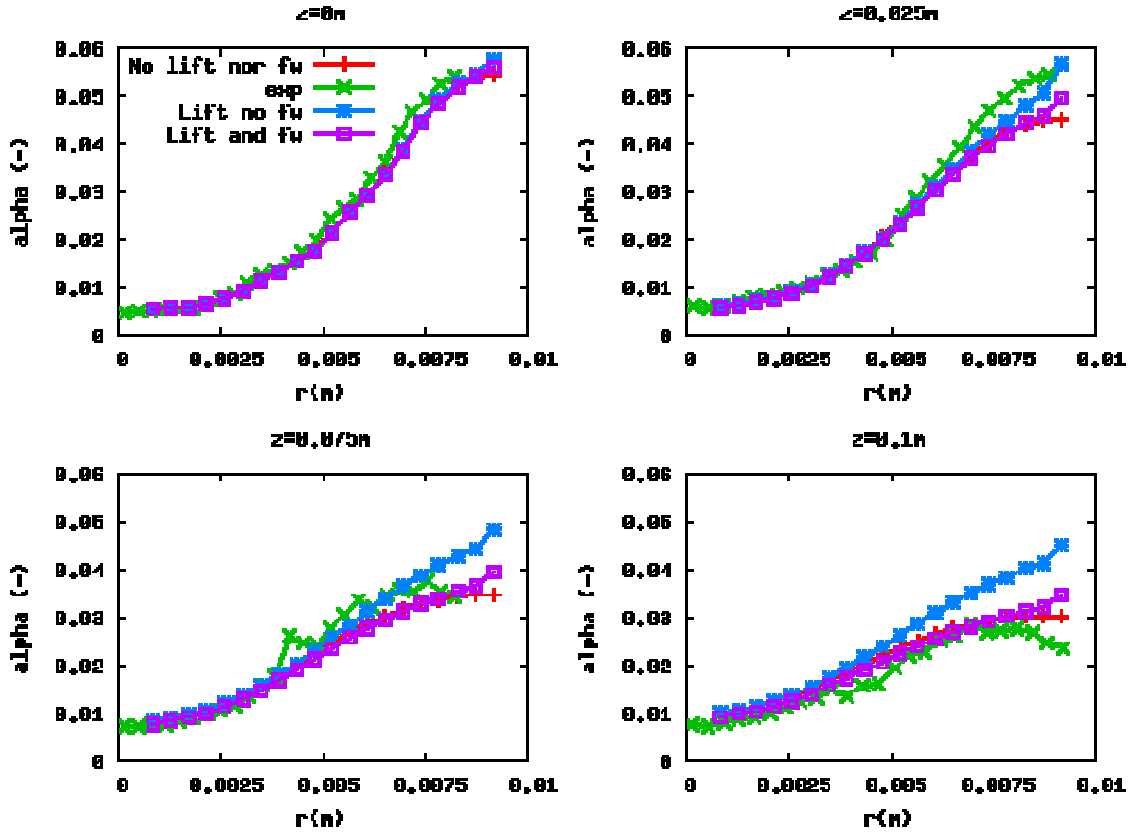

Fig. 4 : Comparison of radial vapour volumetric fraction profiles: experimental data *vs* numerical results for several choices for the closure of the interfacial momentum transfers

In Fig. 4, the vapour volumetric fraction radial profiles at several pipe elevations have been plotted from experimental data and from numerical results for different closures for the interfacial momentum transfers. The thermodydraulic conditions correspond to test1 of Table 2. We clearly identify in all the cases an increase in the centre of the tube along the flow, and a decrease near the wall that we already discussed. In all the cases, the values in the radius range [0:0.004] are very similar. The main differences lie in the shape of the profile in the near wall region. In the experimental case, we observe

that the peak of the void fraction moves from the wall at z=0m or z=0.025m toward the centre whereas it is not the case in the numerical cases.

Let us now consider the case where the lift force is taken into account to balance the turbulent dispersion, but not the wall force. This corresponds to the blue curve “lift” in Fig. 4. This leads to an overestimation of the vapour volumetric fraction, in particular in the near wall region. Indeed, in this region, due to wall shear stress, the lift force is the most intense and this limits the migration toward centre of the pipe where cold liquid could condense them. The overall condensation is thus lower in this case in comparison with the other choices. It is therefore clear that the bubble dynamics, that governs the migration across the pipe section, plays an important role in the condensation dynamics.

To correct this dynamics in the near wall region, let us introduce the wall force, see the purple curve “lift and fw” on the same graphs. This force actually contributes to the migration of bubbles toward centre and thus condensation is more important than in the previous case. This turns out to be insufficient to inverse the wall peak of the profile of α_G in particular for the elevation z=0.1m.

The red curve “no lift or fw” correspond to the case where neither lift nor wall force are taken into account. The profile is in better agreement with the experimental one for the first three elevation. The peak displacement is not reproduced in particular as it can be seen at z=0.1m for the near wall region (r>0.075m).

As a partial conclusion, we analyzed the radial profile of the vapour volumetric fraction and observe

- a large sensitivity of the near wall void fraction profile to the closure of bubbles dynamics, the experimental displacement of the peak cannot be reproduced by the set of classical closure laws, for which we identified a lack of valid correlation for wall force.
- Moreover there is a coupling between bubble dynamics and condensation : lower migration toward the centre of the pipe implies lower condensation.
- whereas in the part of the section closest to the centre, the prediction are *(i)* less sensitive and *(ii)* close to the experimental trends.

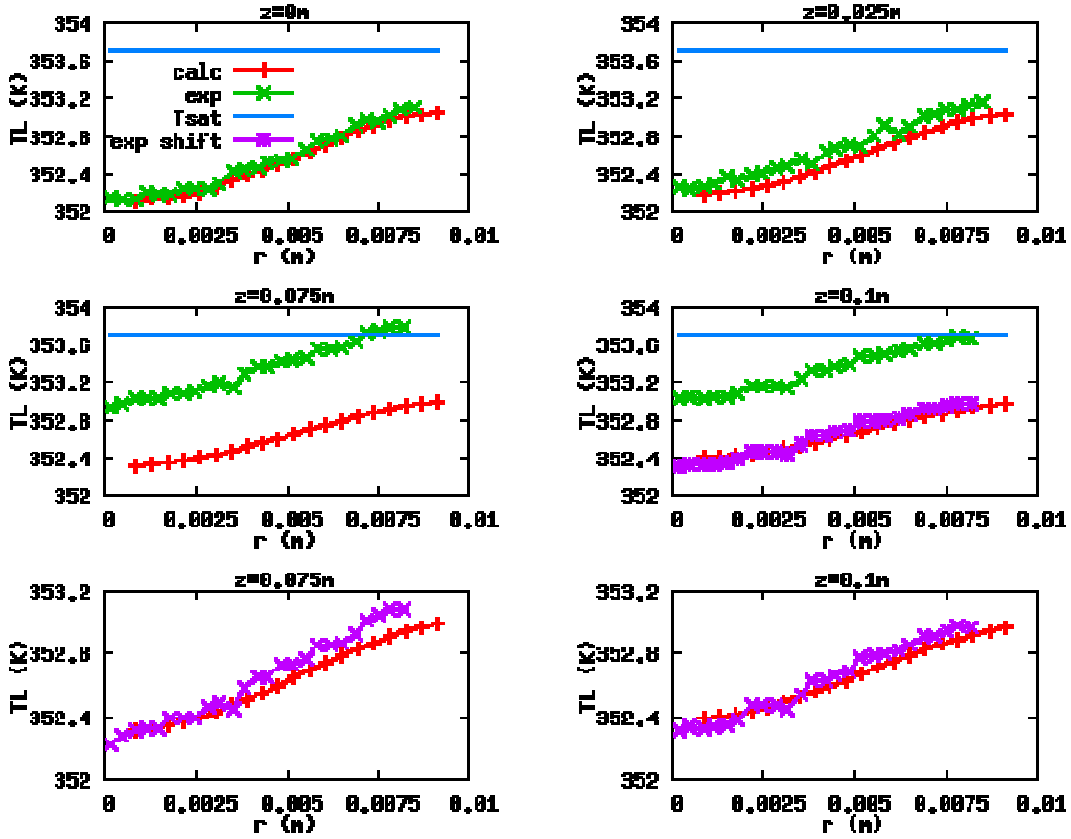

Fig. 5 : Liquid temperature as a function of radial position

4. 4 Liquid temperature

We now consider the comparison between calculated and experimental liquid temperature radial profiles at the different elevations for the thermal-hydraulic conditions of test1 (*cf.* Table 2). It is worth pointing out that the liquid temperature is one of the main physical parameters to address condensation in a bubbly flow: firstly, through its shift from saturation temperature, it governs condensation rate, secondly through its increase throughout the flow it indicates the amount of heat released to the liquid thanks to condensation. The corresponding curves are reproduced in Fig. 5. At the inlet of the calculation domain, the liquid temperature is larger in the near wall region and the difference between the centre and the peak at wall is around 1K. The evolution of the calculated liquid temperature corresponds to an increase of the mean liquid temperature and to a flattening of the profile. Along the 10cm of pipe length considered, the liquid temperature near the wall decreases of about 0.1K, whereas at the centre, it increases of about 0.3K. The global increase is directly related to the condensation heat transfer that heats up the liquid, the flattening being related to thermal diffusion across the pipe diameter. Comparison with experimental data is made in the first two lines of graphs of Fig. 5. The agreement is poor for the two elevations z=0.075m and z=0.1m. On these graphs, the saturation temperature for the given pressure level is given. The experimental values have been shifted adequately on the graphs of the last line of this figure to compare the relative variations between wall and centre of the pipe. It shows that this trend is common to both experimental and numerical results. The interfacial liquid enthalpy is the saturation one for the results that we present and we observed no significant variation in the case where it is modelled as $H_L^I=H_L(T_L,p)$. The bad result concerning the evaluation of the evolution of the liquid temperature level needs to be more deeply studied. Since simulated and experimental vapour volumetric fraction are in agreement for this case, this shift can not been explained by a difference in the condensation rate and reasons of disagreement have not been clarified till now.

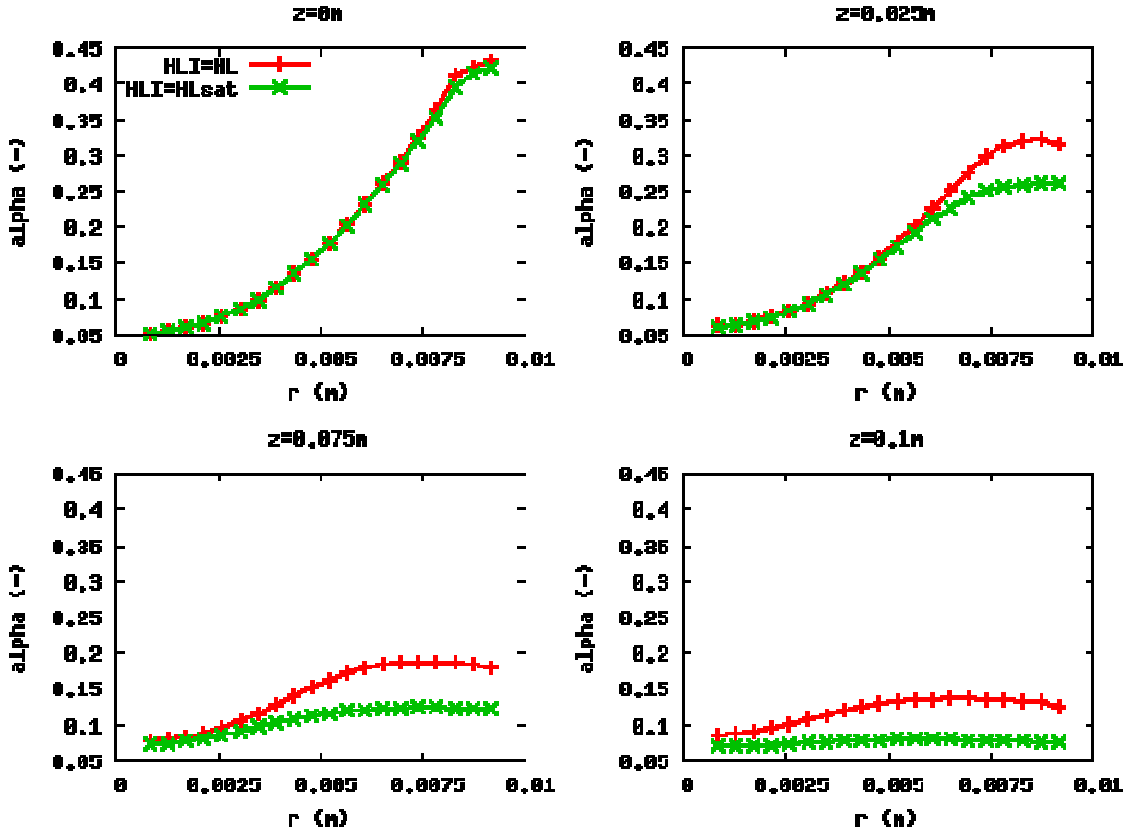

Fig. 6 : Vapour volumetric fraction for two different hypothesis concerning interfacial enthalpy

4.5 Sensitivity to the modelling for interfacial liquid enthalpy

In this calculation, we consider a high subcooling of the liquid phase of 25K at the inlet plane z=0m. Conditions correspond to the data of the test 2, but where liquid temperature is artificially kept at very low level after the heated part. In this case, the hypothesis concerning the interfacial enthalpy of the liquid should have a strong effect on the condensation dynamics. Indeed if we consider the relation between condensation rate and interfacial enthalpy (Eq. 9), the ratio $(H_L^I-H_{Lsat})/(H_{Gsat}-H_{Lsat})$ varies from 0 to 0.25 between the two extreme cases described in section 3. For information, it varied between 0 to 0.03 in the conditions of the test case 1. In Fig. 6, we represent two different calculations corresponding to these two extreme cases. The condensation is stronger in the case where the interfacial enthalpy of the liquid is the saturation enthalpy. The differences between the two vapour volumetric fraction at elevation 1m clearly demonstrate the typical order of magnitude of sensitivity of the result to this modelling for such high subcooling level. For this type of flow, it would be difficult to discriminate the effect on condensation rate between the modeling of *(i)* interfacial enthalpy transfer on the liquid side and *(ii)* interfacial enthalpy.

5. CONCLUSIONS

This work has been devoted to the study of the condensation of convective bubbly flows in the context of nuclear safety studies concerning boiling flows through sub-assemblies. We have introduced the problematic of validation of the CFD code and showed how it requires some dedicated experimental database, in particular for the condensation process.

We have shown that the TESS facility provides some interesting and finely resolved data concerning the condensation dynamics thanks to a dedicated conception of the loop and adequate instrumentation. In order to simulate the condensation dynamics, these data need to be complemented by established liquid velocity and turbulence profiles otherwise the numerical results are not usable for comparison purpose. Development of experimental measurements technologies allowing to access these quantities in a bubbly flow are currently under study, in particular at CEA Grenoble.

We underlined the main sensitivities of the results to some modelling issues. Bubble migration toward centre of the pipe where liquid is colder is one of the key issue since bubbles are initially mainly near the wall and since condensation rate is maximal at mid-position between wall and centre. The quantity of bubbles near the centre is well reproduced by the current models, but the prediction of the migration of the peak of the void profile from wall toward centre is very sensitive to the closure of the bubbles hydrodynamics, in particular the balance between lift, turbulent dispersion, and wall forces. We also underline the impact of the choice for the interfacial liquid enthalpy, as far as high liquid subcooling processes are concerned.

Therefore, it is worth pointing out that the validation of the CFD on convective bubbly flows not only relies on the choice for the liquid interfacial heat transfer but also on the modelling of bubbles hydrodynamics and interfacial liquid enthalpy.

At the current point of this study, main features of the flow have been analyzed, and difficulties concerning the numerical setting of the calculation and sensitivity have been revealed. The next step will then consist in a more extensive validation study against the whole database of the TESS program.

REFERENCES

Auton T. R., “The lift force on a spherical body in a rotational flow”, *J. Fluid Mech.*, Vol. 183, 199-218, (1987)

Basu N., Warrier G. R., Dhir V. K., “Wall heat flux partitioning during subcooled flow boiling; Part 1-Model Development”, *J. of Heat transfer*, Vol. 127, 131-140, (2005)

Cubizolles G., “Etude stéreologique de la topologie des écoulements diphasiques à haute pression”, *phD thesis of Ecole Centrale de Lyon*, (1996)

Gnemmi M., Mangialomini N., François F., “Rapport d’essais DEBORA TESS”, *Technical report CEA DEN/GRE/DTN/SE2T/LTGD/NT/2008-26/C*, (2008),

Guelfi A., Bestion D., Boucker M., Boudier P., Fillion P., Grandotto M., Hérard J.-M., Hervieu E., and Péturaud P, NEPTUNE, "A new software platform for advanced nuclear thermal hydraulics." *Nuclear Science and Engineering*, 156:281-324, (2007)

Ishii M., "Two-fluid model for two-phase flow". *Multiphase Science and Technology*, Hewitt G.F., Delhaye J.M., Zuber N. Eds., Vol. 5, pp. 1-58, (1990).

Ishii M., Hibiki T, Thermo-fluid dynamics of two-phase flow, Ed. Springer., (2006)

Lance M, Lopez De Bertodano. M., "Phase distribution phenomena and wall effects in bubbly two-phase flows." G.F. Hewitt, J.H. Kim, R.T. Jr. Lahey, J.-M. Delhaye and N. Zuber, editors, Begell House, (1994)

Morel Ch., Ruyer P., Seiler N., Laviéville J.-M., "Comparison of several models for multi-size bubbly flows on an adiabatic experiment", *Int. J. Multiphase Flow*, Vol. 36, 25-39 (2010).

Morel Ch., Laviéville J., 2008, Modeling of multi-size bubbly flow and application to the simulation of boiling flows with the NEPTUNE_CFD code, *Science and Technology for Nuclear Installations*, Volume 2009, Article ID 953527. doi:10.1155/2009/953527 (2009)

Ranz, W.E., Marshall, W.R., "Evaporation of drops", *Chemical Engineering Program*, 48, 173-180, (1952).

Tomiyama A., "Struggle with computational bubble dynamics", ICMF'98, 3rd Int. Conf. Multiphase Flow, Lyon, France, pp. 1-18, June 8.-12. (1998)

Zuber N., "On the dispersed two-phase flow in the laminar flow regime", *Chem. Eng. Sc.*, No. 19, p. 897, (1964).